Biogenic supported lipid bilayers as a tool to investigate nano-bio interfaces

Journal of Colloid and Interface Science 570 (2020) 340–349

Contents lists available at ScienceDirect

Journal of Colloid and Interface Science

journal homepage: www.elsevier.com/locate/jcis

Biogenic supported lipid bilayers as a tool to investigate nano-bio interfaces ☆

Costanza Montis [a,1,*], Annalisa Salvatore [a,1], Francesco Valle [b], Lucia Paolini [c], Francesco Carlà [d,e], Paolo Bergese [c], Debora Berti [a]

[a] Department of Chemistry, University of Florence and CSGI, via della Lastruccia 3, 50019 Florence, Italy
[b] ISMN-CNR and CSGI via Gobetti 101, 40129 Bologna, Italy
[c] Department of Molecular and Translational Medicine, University of Brescia and CSGI, Viale Europa 11, 25123 Brescia, Italy
[d] ESRF, The European Synchrotron, 71 Avenue des Martyrs, 38000 Grenoble, France
[e] Diamond Light Source, Harwell Science and Innovation Campus, Fermi Ave, Didcot OX11 0DE, UK

GRAPHICAL ABSTRACT

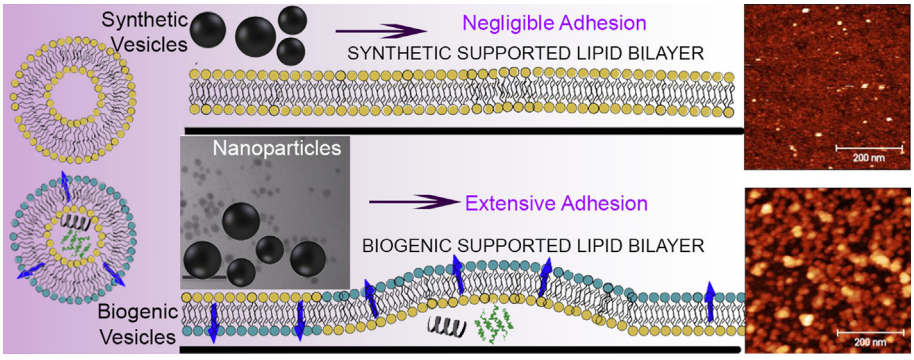

ARTICLE INFO

Article history:
Received 18 December 2019
Revised 3 March 2020
Accepted 4 March 2020
Available online 5 March 2020

Keywords:
Extracellular vesicles
Exosomes
Supported lipid bilayers
SPIONs
Nano-bio interface
Biomimetic membranes

ABSTRACT

Hypothesis: Extracellular Vesicles (EVs) are natural nanosized lipid vesicles involved in most intercellular communication pathways. Given their nature, they represent natural cell membrane models, with intermediate complexity between real and synthetic lipid membranes. Here we compare EVs-derived (EVSLB) and synthetic Supported Lipid Bilayers (SLBs) in the interaction with cationic superparamagnetic iron oxide nanoparticles (SPIONs). The aim is twofold: (i) exploit SPIONs as nanometric probes to investigate the features of EVSLBs as novel biogenic platforms; (ii) contribute at improving the knowledge on the behavior of SPIONs with biological interfaces. **Experiments:** Quartz Crystal Microbalance, X-ray Reflectivity, Grazing-incidence Small-angle X-ray Scattering, Atomic Force Microscopy, Confocal Microscopy data on SPIONs-EVSLB were systematically compared to those on SPIONs challenging synthetic SLBs, taken as references. **Findings:** The ensemble of experimental results highlights the much stronger interaction of SPIONs with EVSLBs with respect to synthetic SLBs. This evidence strongly supports the hypotheses on the peculiar structure of EVSLBs, with cushioned non-flat areas and extended

☆ the Corresponding Author gave a Young Investigator Perspective oral presentation at the 9th International Colloids Conference, 16–19 June 2019, Sitges, Barcelona, Spain.

* Corresponding author.
E-mail address: montis@csgi.unifi.it (C. Montis).

[1] AS and CM contributed equally as first authors to this work.

https://doi.org/10.1016/j.jcis.2020.03.014

exposed surface; in addition, it suggests that these features are relevant in the response of biogenic membranes to nano-objects. These findings contribute to the fundamental knowledge on EVSLBs, key for their development both as biomimetic membranes, or as platforms for biomedical applications.

1. Introduction

Extracellular Vesicles (EVs) are a heterogeneous population of nanosized lipid vesicles naturally secreted by cells. They enclose proteins, nucleic acids, metabolites and they are emerging as important mediators of inter-cellular signaling [1]. The composition and structure of the EV membrane naturally resemble those of the cell membrane involved in the biogenesis machinery of the EV itself – for example, the subpopulation of EVs named "microvesicles" directly pinch off from the plasma membrane, somehow "sampling" it – and may display protein and lipid structures acting as targeting agents that destine EV to particular cell types and mediates interaction with it. Their aqueous pool contains pockets of biologically relevant information (as miRNAs and proteins) to be delivered to their physiological targets [2–7]. EVs are present in all body fluids and are emerging as key regulators in several normal and pathological phenomena, such as cancer spreading, inflammatory states and sepsis, bacterial infections and biofilms formation [8]. Therefore, they are ideal targets for precision medicine, both from a diagnostic and from a therapeutic standpoint [9–11].

Despite their tremendous potential, fundamental knowledge on EVs is still scarce, particularly from a physicochemical perspective. With sizes typical of the colloidal domain (from tens to hundreds of nanometers), EVs can be considered and treated as colloidal objects [12,13]. A physicochemical approach, which leverages the knowledge and know-how of colloidal science, can be therefore crucial to achieve a thorough understanding of the structural and physicochemical characteristics of EVs, which is necessary for EVs engineering and exploitation for therapeutic and diagnostic purposes in biomedical applications [13].

In a recent study [14] we presented a supported lipid bilayer (SLB) obtained through the spontaneous adsorption, opening and coalescence of EVs from a prostate murine cancer cell line (TRAMP-C2), on a solid support of silicon or borosilicate. This biogenic SLB was structurally and physicochemically characterized in relation to a 1-palmitoyl-2-oleoyl-*sn*-*glycero*-phosphocholine (POPC) synthetic SLB. As briefly sketched in Fig. 1a, we found meaningful peculiarities of EVSLBs with respect to the common synthetic SLBs: first, the presence of multiple species (e.g., nucleic acids and small proteins) in EVs lumen determines the formation of "cushion" areas between the solid support and the lipid membrane, which significantly increase the roughness of the EVSLB; in addition, EVSLBs are characterized by a complex lipid composition, leading to a non-homogeneous lateral structure (and viscoelastic properties) of the membrane; finally, EVSLBs are characterized by the presence of functional membrane associated proteins eventually protruding towards the solution [14].

Besides the fundamental relevance of a 2D-projection of EVs to form a supported lipid bilayer of biological origin, the EVSLB displays an intermediate structural and functional complexity between the cell membrane from which the EVs originate and a fully synthetic biomimetic membrane; therefore, it represents a suitable benchmark to investigate biomimetic interfaces and their interactions with nanostructured materials. In addition, EVSLBs can be an ideal platform for the development of biomedical devices, such as biosensors; to achieve this long-term aim, the characteristics of EVSLBs, far from being thoroughly understood, need to be disentangled.

In this study we addressed the interaction of EVSLBs from murine prostate cancer cell lines (TRAMP-C2, from Transgenic Adenocarcinoma of Mouse Prostate model) with superparamagnetic

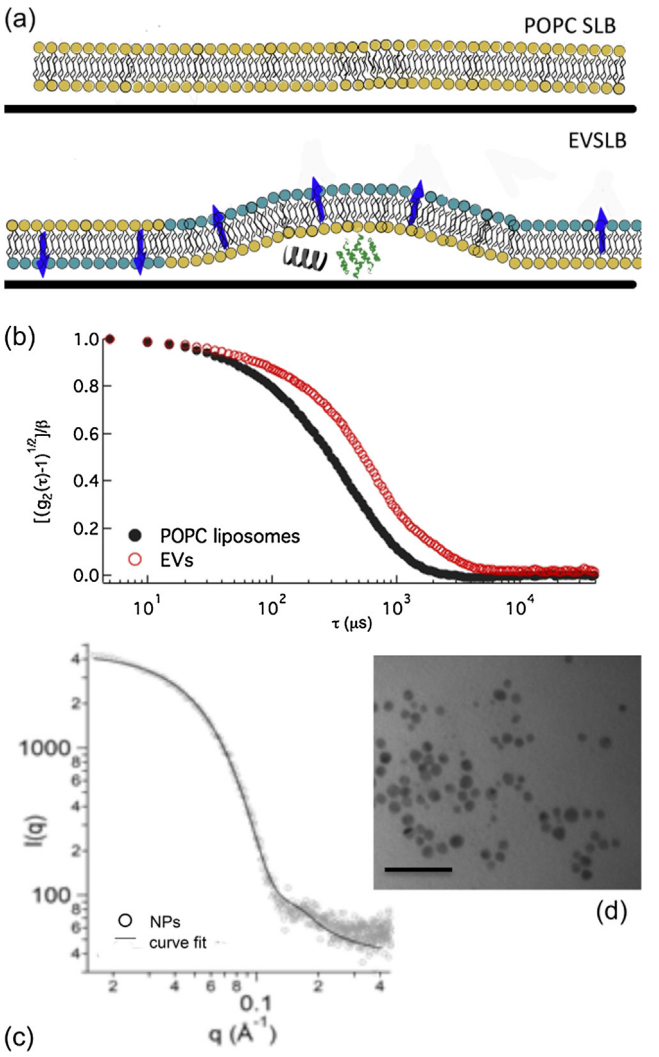

Fig. 1. (a) Sketch of the structural features of EVSLBs and POPC SLBs (readapted from reference [14]): briefly, a synthetic SLB of POPC (upper panel) is made of a single lipid composition (represented by molecules with yellow polar headgroup), low roughness and close interaction with the underlying support; on the other hand EVSLBs (lower panel) are characterized by multiple lipid composition (represented by molecules with yellow or green polar headgroups) and the presence of membrane associated proteins with antigens eventually protruding in the solution (as the blue arrows in the figure) and nucleic acids and proteins originally located in the core of the vesicles, which might remain trapped between the lipid layer and the support, as a cushion, increasing the EVSLBs roughness and decreasing their interaction with the support; (b) representative normalized DLS curves measured for TRAMP-C2 EVs (red empty markers) and POPC liposomes (black filled markers) aqueous dispersion; (c, d) representative SAXS profiles (c) and TEM image (d) of core–shell SPIONs.

iron oxide nanoparticles (SPIONs) coated with a gold shell and a cationic capping agent. SPIONs are among the most investigated nanoparticles for applications in Nanomedicine, e.g. hyperthermia, controlled release and Magnetic Resonance Imaging (MRI). Combining several experimental techniques (QCM-D, X-ray Reflectivity (XRR), Grazing-incidence Small-angle X-ray Scattering (GISAXS), liquid AFM, Confocal Laser Scanning Microscopy (CLSM), we compared the interaction of SPIONs with EVSLBs to the behavior of synthetic SLB from POPC, challenged with the same nanoparticles. This comparison provided information on the phenomena occurring at the nano-bio interface, improving our fundamental knowledge relevant to understand the fate of SPIONs in living organisms. Moreover, nanoparticles (NPs) can be considered as nanoscale probes, which match some of the characteristic lenghtscales of SLBs and EVSLBs (for instance the thickness); therefore, comparing the structural responses of SLBs and EVSLBs to NPs will allow deepening our physicochemical insight into EVSLBs and better understand their structure/response at the nanoscale.

2. Materials and methods

2.1. Materials

Dulbecco's Phosphate-Buffered Saline with 5 mM/L $MgCl_2$, Fetal Bovine Serum, Penicillin-Streptomycin, Glutamine and Dulbecco's Modified Eagle's Medium were purchased from Euroclone. 1-palmitoyl-2-oleoyl-*sn-glycero*-3-phosphocholine (POPC) (≥98.0%), NaCl (≥99.5%), $CaCl_2$ (99.999%), were provided by Sigma-Aldrich (St. Louis, MO). β-BODIPY™ FL C5-HPC (2-(4,4-Difluoro-5,7-Dimethyl-4-Bora-3a,4a-Diaza-s-Indacene-3-Pentanoyl)-1-Hexadecanoyl-snGlycero-3-Phosphocholine) (Bodipy), was purchased from Invitrogen (Invitrogen (Carlsbad, CA). All solutions were prepared with ultrapure water obtained from MilliQ Reference System (Millipore). Cell line: Murine prostatic tumor TRAMP-C2 (ATCC CRL-2731; tissue: prostate; cell type: epithelial) cell line was a gift from Prof. Marco Presta from the Pathology Lab, University of Brescia, Italy, details on cell culture are reported in the SI.

2.2. Preparation of POPC and EVSLB

POPC vesicles For POPC SLB, first POPC vesicles were prepared, according to an established protocol [15]: the proper amount of POPC was dissolved in chloroform/methanol 6:1 (v/v). A lipid film was obtained by evaporating the solvent under a stream of nitrogen and overnight vacuum drying. The film was then swollen and suspended in warm (50 °C) aqueous solution containing 100 mM NaCl by vigorous vortex mixing and then tip-sonicated for 30 min. POPC vesicles were characterized through Dynamic Light Scattering (details on the technique are reported in the SI).

Extracellular Vesicles EVs were isolated and purified according to an established procedure [16], reported in the SI, a final centrifugation step at 100,000g for 4 h (Optima XP80, TY45i rotor, polycarbonate tubes 355,622 Beckmann) allowed obtaining an EV pellet. EVs were characterized for their biochemical composition by western blot analysis of different EV biomarkers (Alix, Annexin XI, TSG101, HSP70, Annexin V, CD81) and a negative control marker (Calnexin) as previously shown in Montis et al. [14]. Purity assessment of EV preparation was determined with the Colorimetric Nanoplasmonic assay as previously described [13,14,17], exploiting the nanoplasmonic properties of colloidal gold nanoparticles and their peculiar interaction with proteins and lipid bilayers [18,19]. Results reported in Fig. S1 showed that the mean *Aggregation Index* (AI) of the EV preparation derived from TRAMP-C2 medium is below 20% of the AI of the starting assay (monodispersed gold nanoparticles, AuNPs). This indicates that EV samples contain negligible amount of protein contaminants. For Dynamic Light Scattering analysis EVs were diluted with a 100 mM NaCl aqueous solution, up to a total vesicle concentration ranging from 10 nM to 50 nM. The EV dispersions in NaCl 100 mM were then equilibrated at 4 °C for 24 h prior to use. EVs were, then, characterized through Dynamic Light Scattering (details on the technique are reported in the SI).

Supported Lipid Bilayers SLBs were prepared by adding 10 mM $CaCl_2$ to the vesicles' dispersion and subsequently depositing a droplet of the vesicles dispersion on a silicon wafer previously polished and activated in a plasma cleaner. A stable SLB layered on the support was obtained by rinsing the vesicles' dispersion with pure milliQ water, after incubation of the vesicles with the support for 20–30 min at r.t. (or 25 °C in the case of QCM-D measurements).

2.3. Synthesis of core–shell nanoparticles

The NPs have been synthesized according a well established protocol, which is extensively reported in the SI [20]: briefly, 2 mmol $Fe(acac_3)_3$ were dissolved in 20 ml phenyl ether containing 6 mmol oleic acid and and 4 mmol oleylamine. 10 mmol 1,2-hexadecandiol were then added. The solution was heated to 210 °C, for 2 h and then cooled to room temperature. The gold shell was formed by mixing 10 ml of the phenyl ether reaction solution of Fe_3O_4 nanoparticles with 2.2 mmol $Au(OOCCH_3)$, 12 mmol 1,2-hexadecanediol, 1.5 mmol oleic acid, 6 mmol oleylamine in 30 ml of phenyl ether. The reaction solution was heated to 180–190 °C for 1.5 h. After cooling to room temperature, ethanol was added. A dark purple material was precipitated and separated by centrifuging. The precipitated product was washed with ethanol, and dispersed in hexane. To get cationic functionalized nanoparticles $Au@Fe_3O_4$ 100 mg of NPs capped with oleic acid and oleylammine and 150 mg of N,N,N-trimethyl(11-mercaptoundecyl)- ammonium bromide were mixed in 20 ml of degassed tetrahydrofuran under nitrogen for two days at room temperature. The black precipitate of the gold nanoparticles was purified by repeated suspension, centrifugation, and decantation with dichloromethane. The NPs obtained were then dissolved in pure water without the need for pH adjustment. The concentration of the obtained solution was. 0.011 mg/mL Fe_3O_4. Core-shell SPIONs were characterized through Small Angle X-ray Scattering, Transmission Electron Microscopy and UV–vis spectroscopy (details on the techniques are reported in the SI).

2.4. Quartz Crystal Microbalance with dissipation monitoring (QCM-D)

QCM-D experiments were performed on a Q-Sense E4 instrument (Q-Sense, Gothenburg, Sweden) in the Partnership for Soft Condensed Matter Laboratory (PSCM) Grenoble (France) [21–23]. The instrument was equipped with four flow liquid cells (0.5 ml internal volume), each containing a coated quartz sensor with 4.95 MHz fundamental resonance frequency, mounted horizontally. The active surface of the sensors (~1 cm^2) was coated with a thin SiO_2 layer (~100 nm thick). The sensors were cleaned prior to use as described in the SI, as well as the experimental details. In QCM-D experiments the vesicles, after a stable baseline was obtained, were injected at 0.1 ml/min flow rate, until a variation of frequency shift and dissipation was detected; then, the vesicles (liposomes or EVs) were incubated with the support in the absence of flow, until a stable adsorption line was detected; subsequently, the layer was extensively washed with milliQ water (at 0.1 ml/min flow rate) to promote the opening/coalescence of vesicles in contact with the support and remove the weakly adsorbed vesicles, until a stable layer was obtained; finally, an appropriate amount of SPIONs stock solution was injected at 0.1 ml/min flow rate, to

completely fill the measurement chamber; after 20 min interaction in the absence of flow, the layer was extensively washed with milliQ water (at 0.1 ml/min flow rate) to promote detachment of weakly adsorbed SPIONs.

2.5. X-ray reflectivity (XRR)

XRR experiments were performed at the ID03 surface diffraction beamline of the ESRF (Grenoble). The experiments were conducted using the six-circles diffractometer (vertical scattering geometry) of experimental hutch 1. The Si substrates used for XRR experiment had an area of about 1×1 cm^2, during the experiment a drop of buffer solution was kept on the sample surface. In order to penetrate the liquid drop with an acceptable loss of intensity an energy of 24 keV, in this condition a water drop with a 1 cm diameter has about 60% transmission. The beam has been focused using a toroidal mirror down to a beam size of 45x600 μm^2 (vxh) at the sample position and a 70×60 μm^2 (vxh) at the GISAXS detector position (1815 mm from the sample position) [24,25]. The images were collected using a Maxipix camera (ESRF) camera (2×2 chips, 516×516 pixels) at a distance of 772 mm from the sample. The software MOTOFIT was employed for the analysis of the XRR curves. A five-layer model was employed to analyze the reflectivity profiles of neat EVSLBs, with scattering length density values calculated for each layer: a bulk subphase of Si, a superficial layer of SiO_2; a second layer of hydration water; a third layer composed of the polar headgroups of the SLB of the inner leaflet; a fourth layer composed of the bilayer lipid chains; a fifth layer composed of the polar headgroups of the outer bilayer leaflet; a bulk superphase of solvent. For POPC SLB a seven-layer model was applied (where the two monolayers of the bilayer lipid chain are separately considered, and an additional layer related to the region of the methyl groups of the bilayer is considered). The scattering length density values for the polar headgroups and lipid chains, which were estimated by taking into account the chemical compositions and the submolecular fragment volumes of phosphatidylcholines as determined by Armen et al. through molecular dynamic simulations [26]. The SLD values of the polar headgroup and the chain of the lipids were then considered as fitting parameters and varied, to take into account of possible SLD variations due to solvent penetration or due to presence of SPIONs. Details on samples preparation are in the SI.

2.6. Grazing-incidence Small-angle X-ray Scattering (GISAXS)

The GISAXS experiment were performed along the XRR experiment at the ID03 beamline, the experimental conditions, in terms of beam energy and beam size, have been kept the same for both kinds of experiment. The beam was focused horizontally at the GISAXS detector position and vertically at the sample position. A Pilatus 100 K-W detector (Dectris) positioned at a distance of 1815 mm from the sample position was used for the GISAXS experiment. A beamstop (500 μm thick Ta foil) was mounted on a motorized stage in front of the GISAXS detector. The GISAXS images were plotted in q-space using Gnuplot, the 1D line cuts along the q_z direction reported below any GISAXS plot were obtained by summing the intensities in the interval $0.015 < Q_z < 0.025$ (as indicated by the dashed line in the Q_y/Q_z plots).

2.7. Atomic force microscopy liquid imaging (AFM)

AFM experiments were always done in liquid, imaging was performed at the SPM@ISMN facility in Bologna [27,28] using a Multimode VIII (Bruker, Santa Barbara, CA, US) and at the Partnership for Soft Condensed Matter (PSCM) in Grenoble using a Cypher S (Asylum Research, Santa Barbara, CA, US). In the first case images were collected in peakforce tapping using SNL Bruker cantilevers with nominal spring constant of 0.24 N/m and 2–10 nm curvature radius, in the second one Olympus BL-AC40TS cantilevers were chosen to perform tapping mode imaging. Images were processed with Gwyddion (D Nečas & P Klapetek. "Gwyddion: an open-source software for SPM data analysis, by simply plane-fitting. SLBs and SLBs + SPIONs were prepared according to the previously described protocol.

2.8. Confocal laser scanning microscopy (CLSM)

To obtain fluorescently-labeled SLBs, a protocol described in the SI was adopted. Fluorescently labeled SLBs on borosilicate coverglasses were obtained according to a similar protocol as that described for X-ray Reflectivity measurements. CLSM experiments were carried out with a laser scanning confocal microscope Leica TCS SP8 (Leica Microsystems GmbH, Wetzlar, Germany) equipped with a 63x water immersion objective [29]. The 488 nm laser line was employed to detect Bodipy fluorescence (λ excitation 488 nm, λ emission 498 nm−530 nm); the samples were visualized both in fluorescence and in transmission mode.

3. Results

Fig. 1b compares the normalized intensity autocorrelation functions of extracellular vesicles from TRAMP-C2 cells, obtained through Dynamic Light Scattering (DLS), with those obtained for synthetic liposomes of 1-palmitoyl-2-oleoyl-*sn*-*glycero*-phosphocholine (POPC), prepared as described in the experimental section. In agreement with the literature [17], the decay profile highlights a slightly larger size and polydispersity of the EVs. Consistently with the literature [30,31], EVs and POPC liposomes are characterized by mildly negative zeta potential, of −18 ± 8 mV and −9 ± 3 mV for EVs and POPC vesicles, respectively. Thanks to a protocol described in the Materials and Methods and reported in a previous publication, the vesicles, dispersed in a 0.1 M NaCl aqueous solution and additioned with 10 mM $CaCl_2$, were put in contact with borosilicate or silicon supports to form a 2D *replica of the membrane*, where a supported lipid bilayer completely covers the surface. These systems, whose different structural features have been previously elucidated (see Fig. 1a), were then challenged with an aqueous dispersion of SPIONs. Core-shell SPIONs were synthesized according to a well-established procedure (see Materials and Methods), leading to slightly polydisperse nanospheres with average diameter of 6 nm (see TEM image, Fig. 1d and SAXS characterization, Fig. 1c). The particles were coated by a gold shell, whose presence was confirmed by with UV–vis absorbance (see SI Fig. S2); SAXS curves were analyzed with a polydisperse core–shell model, yielding an average core diameter of 4.2 nm and shell thickness of around 0.9 nm; the NPs were functionalized with a positively charged ligand (N,N,N-trimethyl(11-mercaptoundecyl)-ammonium bromide), which imparts a positive zeta potential (+27 ± 3 mV).

Fig. 2 displays the QCM-D results, monitoring the formation of a SLB for EVSLB (Fig. 2a) and POPC SLB (Fig. 2b), and the interaction with cationic core–shell SPIONs.

At t = 0 both TRAMP-C2 EVs and POPC liposomes in NaCl 0.1 M are injected in the measurement chamber: the adsorption of the vesicles on the silicon support, which is favored by the presence of Ca^{2+} ions in solution, is clearly visible as a strong increase (in absolute value) of both the frequency shift and the dissipation factors (see Fig. 2a, b time range 0–2000 s); then, upon rinsing with water [14], all the weakly interacting vesicles are removed and the opening and coalescence of the vesicles adsorbed on the support is promoted, resulting in the concomitant decrease of both

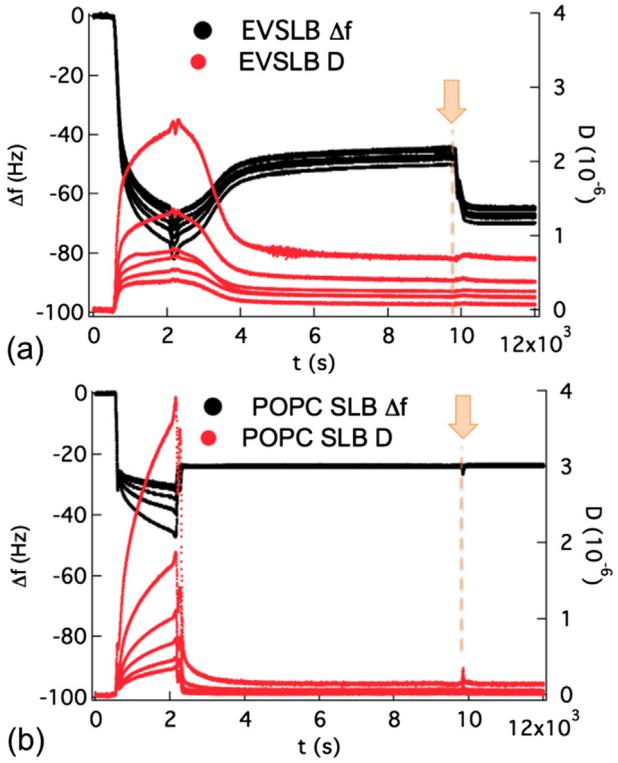

Fig. 2. QCM-D curves monitoring the formation of (a) EVSLB and (b) a POPC SLB through vesicle fusion. Both the frequency shifts (black markers) and the dissipation factors (red markers) of the different overtones (3rd, 5th, 7th, 9th, 11th, 13th) are reported. Upon the formation of the SLB an aqueous dispersion of cationic SPIONs is injected in the measurement chamber: the injection of SPIONs is in both graphs highlighted by an orange arrow and an orange dashed line.

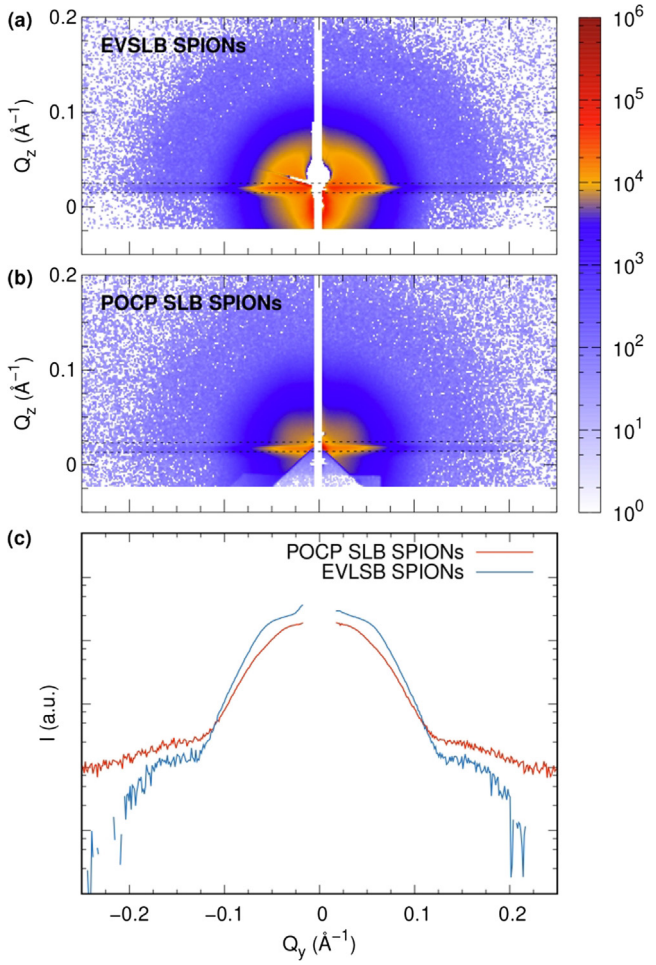

Fig. 3. GISAXS patterns of (a) EVSLB upon incubation with SPIONs and (b) POPC SLB upon incubation with SPIONs. The GISAXS signal has been measured before and after the incubation with SPIONs and the the 2D plots have been obtained by calculating the difference between the images of the SPIONs containing samples and the ones of the pristine samples; (c) Comparison of GISAXS plots along Q_y obtained for image (a) and (b) by integrating the regions in the interval $0.015 < Q_z < 0.025$ (as highlighted by the dashed lines in the 2D GISAXS 2D images).

frequency shift and dissipation factors, until a stable layer remains, corresponding to a supported lipid bilayer (see Fig. 2a, b time range 2000–10000 s) [14,15]. The structural and compositional differences in EVSLBs and POPC SLBs sketched in Fig. 1a trigger a higher frequency shift, higher dissipation factor and higher spreading of the overtones in the case of the EVSLB compared to the POPC SLB. This is consistent with the model of the EVSLB to be formed by a bilayer, which has a higher roughness (also mirrored by an overall higher adsorbed mass) and less firmly coupled with the supporting surface, with respect to the POPC (in agreement with our previous study [14]).

Subsequently, we injected in the QCM-D chamber an appropriate volume of the aqueous dispersion of core–shell SPIONs (stock solution 0.01 mg/mL Fe_3O_4 amount diluted 1:1) to completely fill the chamber. Interestingly, no major variation are observed in QCM-D profile measured for POPC SLB (see the orange arrow in Fig. 2); on the contrary, a significant amount of SPIONs adsorb on the EVSLBs, as highlighted from the significant frequency shift visible in Fig. 2a, b. Interestingly, as already pointed out, this adsorption takes place without significant modifications in the dissipation factors of the layer, suggesting that, upon NPs adhesion, no significant modifications of the viscoelastic properties of the EVSLB occur.

In order to structurally characterize the SPIONs adhesion to the EVSLB, we exploited surface XRR and GISAXS, which provide information at the nanometer lengthscale on the features of EVSLB before and after incubation with SPIONs, in comparison with POPC SLB.

Fig. 3a, b compares the GISAXS images of EVSLB and POPC SLB in the presence of SPIONs. The displayed images are each subtracted of the corresponding GISAXS image of the SLB in the absence of SPIONs. GISAXS images of the SLBs in the absence of SPIONs do not show significant details, as well as GISAXS image of the SPIONs adsorbed on the bare silicon layer (see SI Fig. S3). Conversely, GISAXS images of both POPC SLB and EVSLB incubated with NPs display a signal at $q_y = 0.17$ Å^{-1}. This value is consistent with the oscillation of the form factor of the nanoparticles (see SAXS profile, Fig. 1c): therefore, the presence of POPC SLB and the EVSLB seems to promote the adhesion of SPIONs on the surface (as already pointed out, the adhesion of SPIONs on the bare silicon wafer is negligible). Interestingly, comparing GISAXS profiles of the EVSLB/SPIONs and POPC SLB/SPIONs along q_y (Fig. 3c), the oscillation on the EVSLB plot appears much more defined than the on the POPC SLB plot. Therefore, we can formulate some hypotheses: (i) Notwithstanding the negligible amount of SPIONs adsorbed on POPC SLB highlighted from QCM-D, from a structural inspection it appears that some adhesion of SPIONs on the synthetic lipid membrane is occurring; (ii) For POPC SLB and EVSLB a similar interaction phenomenon with SPIONs occurs: from GISAXS we observe in both cases the appearance of an oscillation around $q_y = 0.17$ Å^{-1} (due to the form factor of SPIONs), while from QCM-D a high extent of SPIONs adsorption on EVSLB membrane is highlighted. It appears therefore that the SPIONs adsorbed on the EVSLB are, as on POPC SLB, simply adsorbed, with no evidences

of specific correlation distances between them. This can be possibly correlated with the negligible variation of dissipation in the QCM-D profile, suggesting that the NPs adsorb superficially on the EVSLB, without reorganizing themselves in a specific arrangement upon adhesion (GISAXS) and, therefore, without deeply modifying the viscoelastic properties of the layer (QCM-D). (iii) Nevertheless, a higher extent of SPIONs adsorption on EVSLBs with respect to POPC SLBs is highlighted from the comparison of GISAXS profiles displayed in Fig. 3c, confirming the results obtained from QCM-D.

It should be pointed out that the absence of NPs adhesion on POPC SLB as highlighted from QCM-D could be considered in apparent contrast with the evidence of NPs adsorption on POPC SLB as evidenced from GISAXS. A possible explanation of this discrepancy can be provided considering that QCM-D experiment is an in-flow experiment on a vibrating crystal: if a surface interaction between the NPs and POPC SLB occurs, the vibration of the crystal, together with the flow, might synergistically promote the detachment of weakly adsorbed NPs, leaving on the surface a few undetected NPs, which are below the sensitivity of the technique; on the other hand, GISAXS (as well as in the experiments shown in the following paragraphs, i.e., XRR, AFM, CLSM) are batch techniques where the rinsing step is performed on a still, non-vibrating support, where even a weak interaction between NPs and POPC SLB might be slightly more favored. This discrepancy between GISAXS and QCM-D could, therefore, suggests the interaction of SPIONs with POPC SLB is relatively weak and labile.

Fig. 4a displays a representative XRR curve measured for a POPC SLB before and after the addition of SPIONs. In the absence of NPs the bilayer appears relatively homogeneous in thickness, as highlighted by the three clear oscillations; the curve was analyzed with MOTOFIT [32] (the fitting curve is displayed as a continuous line in Fig. 4a), to derive the structure of the bilayer along the z-axis: briefly, as described more in details in the Materials and Methods section and in the SI, through MOTOFIT the SLBs can be modeled as multilayers (comprising a layer for the inner polar headgroup, a layer for the lipid chains and a layer for the outer polar headgroup), each characterized by a thickness, a scattering length density value and a roughness. Consistently with the literature, an overall bilayer thickness of around 4 nm was obtained, with a thickness of the polar headgroup and of the hydrophobic alkyl chain of 0.5 nm and 3.3 nm, respectively (the scattering length density perpendicularly to the bilayer, together with a sketch of the bilayer profile is reported in the inset of Fig. 4a, for XRR curves fitting results see the Table 1). When SPIONs are added to the lipid bilayer, non-negligible differences can be detected, as the profiles' comparison highlights (Fig. 4a). We modeled the reflectivity including an additional layer, with fixed thickness comparable with the SPIONs diameter (6 nm): from the fitting procedure the SPIONs layer resulted characterized by an extremely high roughness (2 nm) and SLD value (10×10^{-6} Å^{-2}, see Table 1) similar to pure water (9.42×10^{-6} Å^{-2}). This SLD is far from the value calculated for SPIONs (around 100×10^{-6} Å^{-2}), which hints at a high hydration degree (99%) of the SPIONs layer, consistent with sparse adsorption.

Fig. 4b (black markers) displays the XRR profile of EVSLB layered on a silicon support. Clearly, the curve appears very different from that measured for POPC. No oscillations are visible, and the profile only slightly differs from the bare silicon surface in water (see SI, Fig. S4, reference curve for Si wafer). The situation changes dramatically when this layer is challenged with SPIONs: while no effects are visible for support (SI Fig. S4), a clear pattern appears measured for EVSLB (Fig. 4b). This evidence, in line with the QCM-D data, confirms that a layer is indeed present on the surface, and that it is probably characterized by a significant roughness, which smears out the curves oscillations with respect to POPC. In

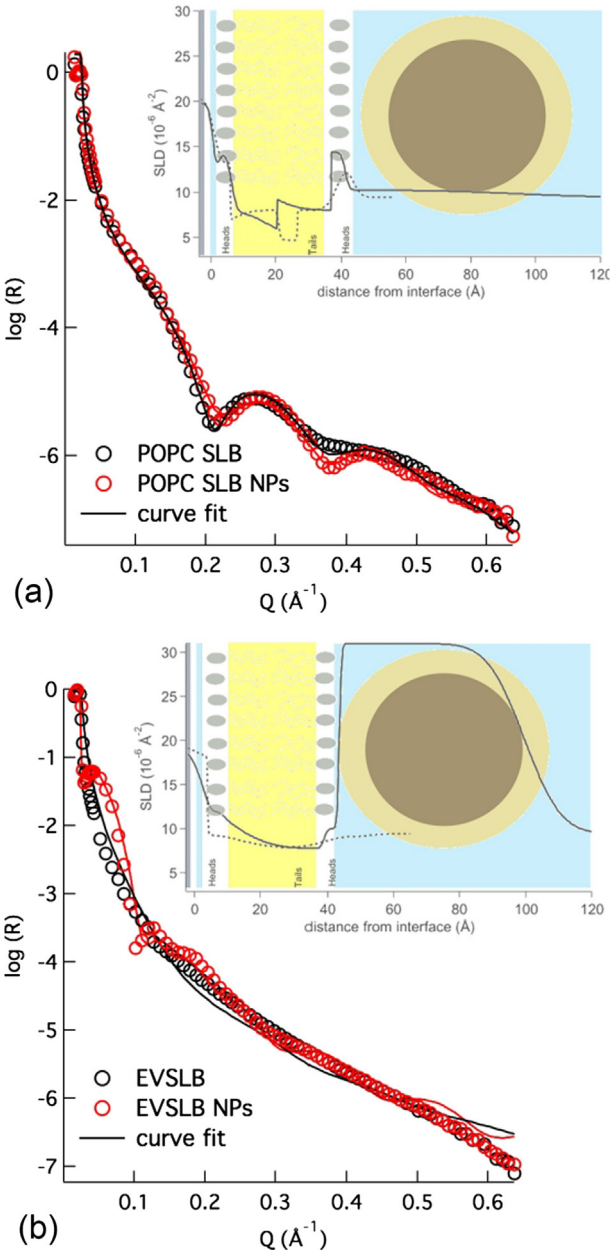

Fig. 4. Representative X-ray Reflectivity profiles of (a) POPC SLB and (b) EVSLB in the absence (black markers) and in the presence (red markers) of SPIONs; fitting curves obtained with MOTOFIT [32] are reported as continuous lines, the corresponding scattering length density profiles perpendicularly to the bilayer are reported in the insets.

spite of the complexity of the EVSLB, the curve could be analyzed according to a similar model as the one applied for POPC SLB, introducing a dramatic increase of the roughness of the layers (see fitting curve, black continuous line in Fig. 4b and fitting parameters in Table 1). If this layer is exposed to SPIONs, a series of oscillations appears at low Q, providing a first qualitative confirmation that the effects of SPIONs on SLBs is much stronger for EVSLB than for POPC. The curve was analyzed with the same model applied for neat EVSLBs (Fig. 4b, red continuous line), with the inclusion of an additional layer, matching the size of SPIONs (see Table 1), which, as expected, is significantly less hydrated (around 76%, corresponding to a SLD of 31×10^{-6} Å^{-2}) than for POPC. This highlights that the adhesion of SPIONs on EVSLB surface is strongly promoted, and that SPIONs form a layer on the lipid membrane, which, on aver-

Table 1
Curve fitting results of XRR data measured for POPC SLB and EVSLB before and after incubation with SPIONs, obtained with MOTOFIT. The reported fitting parameters are referred to the three layers composing the bilayer (Inner Heads, referred to the layer of polar headgroups in contact with the support, Lipid Chains, referred to the hydrophobic region of the SLBs, Outer Heads, referred to the layer polar headgroups in contact with the solvent (i.e., water)); for the SLBs incubated with NPs an additional layer containing SPIONs is considered above (and in contact with) the Outer Heads layer. For each layer three parameters are reported: *d(Å)*, the thickness of the layer; *SLD (10^{-6} Å^{-2})* scattering length density of the layer (SLD were considered as fitting parameters, in order to take into account of solvent penetration effects); *ρ (Å)* roughness of the layer.

Layers		POPC SLB	POPC SLB SPIONs	EVSLB	EVSLB SPIONs
SPIONs	*d(Å)*	–	60	–	60
	SLD (10^{-6} Å^{-2})	–	10 ± 1	–	31 ± 1
	ρ (Å)	–	21 ± 2	–	10 ± 2
OuterHeads	*d(Å)*	4 ± 1	4 ± 1	4 ± 2	5 ± 2
	SLD (10^{-6} Å^{-2})	14.4	14.4	10.2 ± 0.5	10.0 ± 0.5
	ρ (Å)	2 ± 1	1 ± 1	4 ± 2	2 ± 1
Lipid Chains	*d(Å)*	33 ± 4	31 ± 2	31 ± 4	29 ± 3
	SLD (10^{-6} Å^{-2})	7.6	7.6	7.7 ± 0.3	7.7 ± 0.2
	ρ (Å)	3 ± 1	5 ± 2	8 ± 2	2 ± 1
InnerHeads	*d(Å)*	4 ± 1	4 ± 1	6 ± 2	4 ± 1
	SLD (10^{-6} Å^{-2})	14.4	14.4	10.0 ± 0.5	13.8 ± 0.8
	ρ (Å)	1 ± 1	1 ± 1	9 ± 2	2 ± 1

age, affects the whole EVSLB structural profile. Finally, it should be pointed out that for both SLBs the additional layer due to NPs adsorption (to different extents for POPC SLB and EVSLB), does not significantly modify the underlying layers (that is, the polar headgroups layers and lipid chains layers of the SLB), suggesting that the interaction between SPIONs and SLBs is superficial, both for POPC SLBs (where the adsorption of SPIONs is mild) and for EVSLBs (where the adsorption of SPIONs is extensive).

The arrangement of the NPs on the lipid layers and their effects on the SLBs was also addressed with microscopic techniques, namely liquid AFM and CLSM.

First, to visualize the arrangement of the nanoparticles on the two types of SLBs at a nanometer lengthscale, we performed liquid AFM. Representative AFM images are shown in Fig. 5a-c.

In most regions of POPC SLB few nanoparticles are present, as clearly visible in Fig. 5a, while in some limited regions (an example is shown in Fig. 5b) the adsorption of NPs on the SLB appears more effective. On the other hand, the EVSLB appears in all observed regions to be completely covered by SPIONs (Fig. 5c). A dense layer of SPIONs is visibly adsorbed on the SLB of EVs, upon incubation of the EVSLB with SPIONs, which is consistent with the XRR data. On the other hand, only a few NPs adhere on POPC SLB, in agreement with the mild variation of scattering length density of POPC bilayer along the z-axis, upon interaction with SPIONs, highlighted from XRR. The height distribution related to Fig. 5c is reported in Fig. 5d, where three main peaks are indicated by arrows: peak 1 is related to the EVSLB substrate; peak 2, the most intense, is localized at approximately 6 nm from the substrate, therefore, it is clearly related to a first layer of SPIONs (it nicely matches the diameter of SPIONs); finally, peak 3, which is of much lower intensity, is of about 13 nm in height, therefore, it is attributable to the presence of few SPIONs on top of the first layer of nanoparticles adsorbed on the EVSLB.

As a final experiment, we monitored the same interaction through confocal microscopy, on a larger lengthscale: Fig. 6a, 6b display representative CLSM images of a (a) POPC SLB and a (b) EVSLB containing a fluorescent tag (Bodipy, green) in the bilayer. As already shown in a recent publication [14], EVSLBs are characterized by the presence of lateral inhomogeneities within the bilayer, reflecting the higher complexity in structure/composition of the biogenic supported lipid bilayer with respect to the synthetic ones. However, in the absence of SPIONs both types of bilayers appear as relatively homogeneous. Upon addition of SPIONs, a different effect is visible for POPC SLB (Fig. 6c, d) and EVSLB (Fig. 6e-h): upon incubation with SPIONs for POPC SLB a restructuring of the membrane is apparent, leading to the increased inhomogeneity in the distribution of the fluorescent dye within the membrane (Fig. 6c), however, in the same scan field, the transmission image (Fig. 6d) shows the presence of few dark spots, attributable to small and rare SPIONs aggregates. On the other hand, the effect of SPIONs on EVSLBs is much more evident: while the distribution of the lipid dye within the membrane is only mildly affected by the interaction with SPIONs (see Fig. 6e, g compared to Fig. 6b), extended black spots appear in the bright field images (Fig. 6f) and, by increasing the magnification of the scan field (Fig. 6h) it appears that small aggregates are present also at shorter length scales.

4. Discussion

Combining all the experimental results on the interaction of SPIONs with SLBs from EVs and POPC, it is possible to formulate a hypothesis on the nature and main characteristics of the interaction of SPIONs with biogenic SLBs, and to correlate them with the peculiar features of the EVSLBs [14]. Clearly, membrane proteins, which are present in high amount in the EVSLB and completely absent in the fully synthetic SLB, might play an important specific role, which will deserve more detailed studies. Concerning the originating vesicles, EVs and POPC liposomes are both characterized by a mildly negative zeta potential, with slight differences that do not justify such a different interaction pathway with SPIONs. On the other hand, as pointed out in the introduction, there are some specific structural differences of the EVSLB compared to POPC SLB, which have been highlighted in a previous work [14]. First, EVSLBs are characterized by a more complex composition, with the presence of biomolecules and multiple lipid species, which affect: (i) the viscoelastic properties of the EVSLB (detected through a significant spreading of the overtones in QCM-D and concomitant increase of the dissipation, with respect to POPC, see Fig. 2) (ii) the lateral homogeneity (visualized for instance through confocal microscopy, see ref. [14]) (iii) the localized curvature of the membrane, which might not be completely flat. Second, due to different possible opening mechanisms of EVs to form the EVSLBs, upon vesicles opening they can release their cargo either to the side of the aqueous medium or to the side of the support; in this latter case, the biomolecules are trapped between the support ant the SLB, forming a localized cushion; this process determines: (i) an increased roughness of the layer (see AFM data in ref. [14]) and, therefore, (ii) an overall increased surface area exposed to the interaction with SPIONs; (iii) a lower coupling of the layer with the underlying support (as highlighted from QCM-D, Fig. 2), possibly leading to (iv) lower bending energy, both due to a lower interaction of the lipid membrane with the support, and due to the

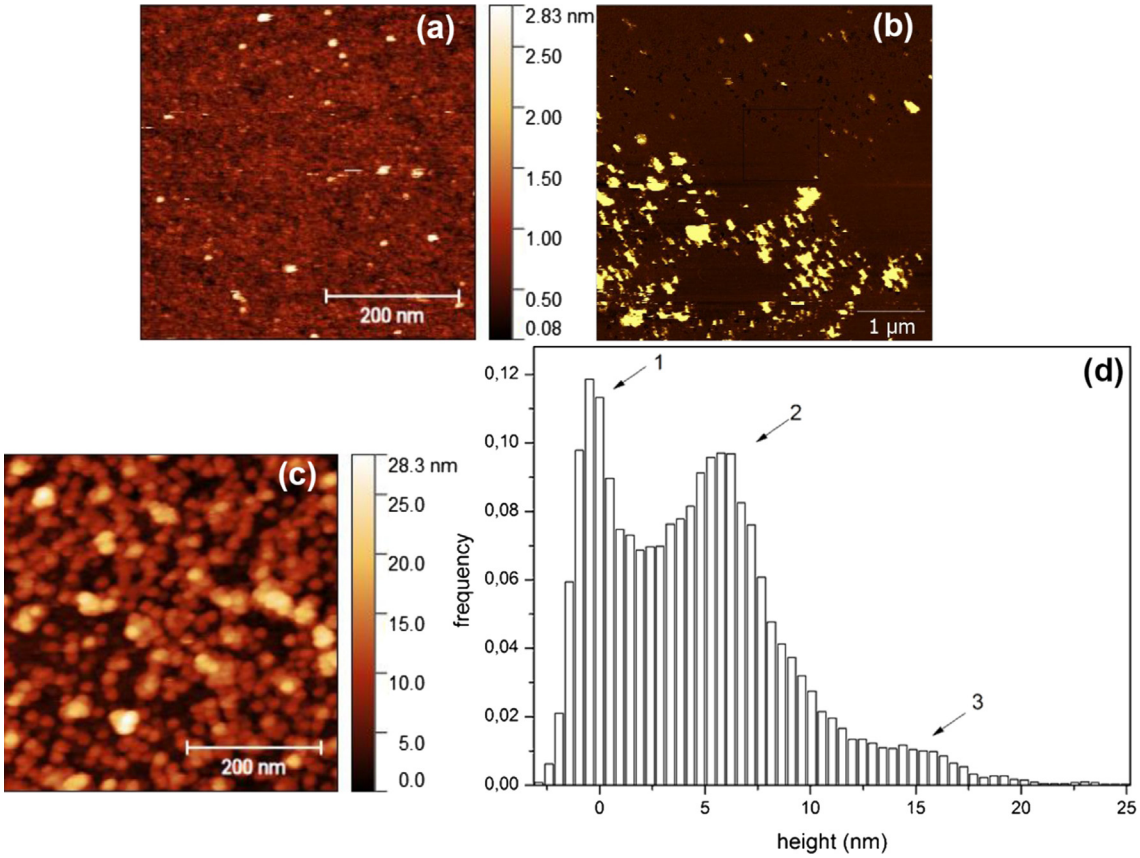

Fig. 5. Representative liquid AFM images of (a, b) POPC SLB and (c) EVSLB, upon incubation with SPIONs. For POPC SLBs panel (a) shows the poor adsorption of SPIONs on the SLB, while panel (b) highlights the presence of areas with SPIONs adsorbed and areas which are completely empty. On the other hand the EVSLB (c) is completely covered by nanoparticles; (d) In the graph the height distribution of the image (c) is reported where three peaks can be visualized and highlighted with arrows; peak 1 is the underlying EV substrate, peak 2 is the first layer at approximately 6 nm and peak 3 is due to the presence of SPIONs on top of the first layer (about 13 nm in height).

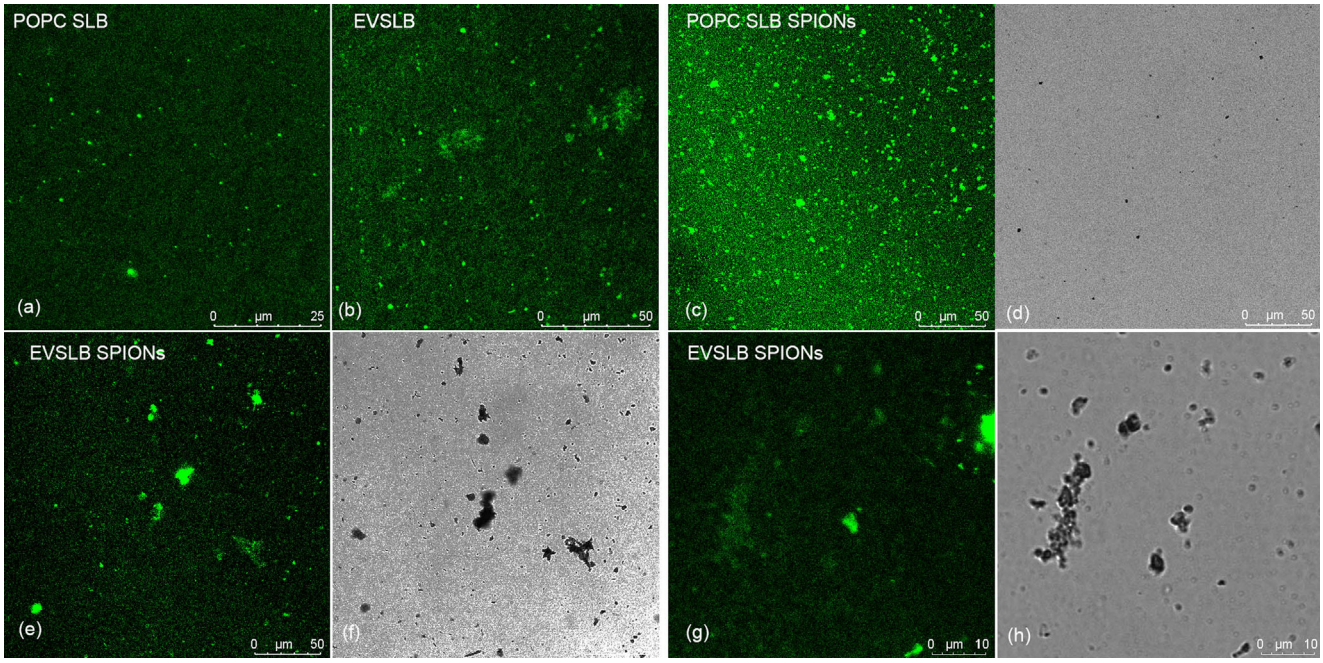

Fig. 6. Representative CLSM images of (a) POPC SLB and (b) EVSLB (fluorescence), (c, d) POPC SLB upon incubation with SPIONs (c, fluorescence, d transmission); (e-h) EVSLB upon incubation with SPIONs (e, g fluorescence, f, h transmission).

presence of localized curved regions, arising from the presence of neighboring cushioned and uncushioned areas of the EVSLB.

Concerning the adhesion of SPIONs to the EVSLBs, the ensemble of the experimental data here shown highlights that: SPIONs tend to interact more effectively with the EVSLBs with respect to POPC SLBs, and that EVSLBs seem to actively recruit SPIONs (see QCM-D, XRR and AFM results), as compared to POPC SLBs. This effect, detected at the nanoscale, seems to determine also more extended phenomena of SPIONs adhesion and clusterization on EVSLBs, as highlighted by Confocal Microscopy images. However, interestingly, this effect of SPIONs recruitment and extensive adhesion on the EVSLB seems to be the result of a relatively superficial interaction, which does not lead to SPIONs in-plane correlation phenomena (GISAXS), affects only mildly the structural features of EVSLB membrane (XRR) and does not modify the viscoelastic properties of the EVSLB (QCM-D).

These data can be understood considering the previously discussed structural features of EVSLBs, in particular: (i) The high roughness of EVSLBs as compared to POPC SLBs clearly determines an increased surface area of the EVSLB, which is exposed to the interaction with exogenous species; (ii) Cushioned areas of the EVSLB, which are less coupled with the underlying support, are more prone to interact with exogenous species, without being hampered by the presence of the support; (iii) The roughness and lateral inhomogeneity of EVSLBs leads to the presence of localized non-flat regions, which are characterized by lower bending energy and are, therefore, more prone to interact with nano-objects, which are known to impose a curvature to lipid membranes upon adhesion [33,34].

Overall, the consistency between the available structural data on EVSLBs and their response to nano-objects, as here discussed, provide additional proofs of the structural and physicochemical features of biogenic EVSLBs, compared to fully synthetic SLBs. In addition, it is highlighted how these structural features are of prominent relevance in determining the response of EVSLBs to nano-objects.

5. Conclusion

In this contribution we have combined different experimental techniques (QCM-D, X-ray Reflectivity, GISAXS, AFM, Confocal Microscopy) to compare the interaction of SPIONs with synthetic and biogenic supported lipid bilayers. We found that the adhesion of SPIONs on lipid membranes is strongly promoted for EVSLBs with respect to synthetic POPC SLBs. This effect, highlighted with all the different techniques, can be rationalized taking into account the higher complexity of EVSLB with respect to POPC SLB, determining a significant roughness of EVSLBs, which leads to: (i) the presence of area of partial detachment from the underlying support, which can more easily bend to interact with an adhering nanoparticle; (ii) the presence of non-flat regions with a localized non-zero curvature, which, again, can more easily bend without energy costs to interact with nanoparticles; (iii) an increase of the overall exposed surface, favoring the interaction with nanoparticles.

Overall, the increased roughness and complexity of EVSLBs with respect to the synthetic SLBs seem to be key in driving a dramatic enhancement in the response to the adhesion of nano-objects. This evidence strongly supports the hypothesized structure of the EVSLB, as described in a recent publication [14], thus strengthening the understanding on the structural and physicochemical features of the EVSLBs, which is of relevance in view of a possible exploitation of these systems as 2D platforms for biosensors applications. In addition, EVSLBs appear as interesting platforms for fundamental studies in colloid and interface science [35–37], to investigate nano-bio interfaces in controlled conditions, allowing exploiting a lipid membrane characterized by intermediate complexity between a fully synthetic lipid membrane and the eukaryotic plasma membrane. Interestingly, the displayed data provide a general hint on the relevance of membrane localized curvature and bending energy in modifying the interactions at nano-bio interfaces, which is consistent with the theoretical predictions [38,39] and with previous experimental studies on supported and free-standing synthetic lipid membranes [34], and might also suggest the relevance of non-flat, curved membrane structures in real cells in the interaction with nano-objects. In the future, a more thorough understanding of EVSLBs will require a full characterization of the embedded biomolecules, with the aim to disentangle their role in the response of EVSLBs to exogenous species and to fully exploit and develop the potential of these novel biogenic platforms.

CRediT authorship contribution statement

Costanza Montis: Conceptualization, Investigation, Methodology, Data curation, Writing - original draft, Supervision. **Annalisa Salvatore:** Investigation, Methodology, Data curation, Writing - original draft. **Francesco Valle:** Investigation, Data curation. **Lucia Paolini:** Investigation. **Francesco Carlà:** Investigation, Methodology, Data curation, Writing - review & editing. **Paolo Bergese:** Funding acquisition, Supervision, Writing - review & editing. **Debora Berti:** Funding acquisition, Supervision, Writing - review & editing.

Acknowledgements

The Partnership for Soft Condensed Matter (PSCM) is gratefully acknowledged for QCM-D and AFM measurements; evFOUNDRY (H2020-FETOPEN-2016-2017—Project ID: 801367) is acknowledged by all authors for a financial support. AFM experiments were performed at the SPM@ISMN microscopy facility in Bologna and at the PSCM, Grenoble with the help of Marie Capron and Alain Panzarella.

Appendix A. Supplementary material

Supplementary data to this article can be found online at https://doi.org/10.1016/j.jcis.2020.03.014.

References

[1] S. Busatto, A. Zendrini, A. Radeghieri, L. Paolini, M. Romano, M. Presta, et al., The nanostructured secretome, Biomater. Sci. 8 (2020) 39–63, https://doi.org/10.1039/C9BM01007F.
[2] G. Raposo, W. Stoorvogel, Extracellular vesicles: Exosomes, microvesicles, and friends, J. Cell Biol. 200 (2013) 373–383, https://doi.org/10.1083/jcb.201211138.
[3] M. Tkach, C. Théry, Communication by extracellular vesicles: where we are and where we need to go, Cell (2016), https://doi.org/10.1016/j.cell.2016.01.043.
[4] S.L.N. Maas, X.O. Breakefield, A.M. Weaver, Extracellular vesicles: unique intercellular delivery vehicles, Trends Cell Biol. (2017), https://doi.org/10.1016/j.tcb.2016.11.003.
[5] G. Van Niel, G. D'Angelo, G. Raposo, Shedding light on the cell biology of extracellular vesicles, Nat. Rev. Mol. Cell Biol. (2018), https://doi.org/10.1038/nrm.2017.125.
[6] M. Mathieu, L. Martin-Jaular, G. Lavieu, C. Théry, Specificities of secretion and uptake of exosomes and other extracellular vesicles for cell-to-cell communication, Nat. Cell Biol. (2019), https://doi.org/10.1038/s41556-018-0250-9.
[7] L. Margolis, Y. Sadovsky, The biology of extracellular vesicles: The known unknowns, PLOS Biol. (2019), https://doi.org/10.1371/journal.pbio.3000363.
[8] J. De Toro, L. Herschlik, C. Waldner, C. Mongini, Emerging roles of exosomes in normal and pathological conditions: New insights for diagnosis and therapeutic applications, Front. Immunol. (2015), https://doi.org/10.3389/fimmu.2015.00203.

[9] S. El Andaloussi, I. Mäger, X.O. Breakefield, M.J.A. Wood, Extracellular vesicles: Biology and emerging therapeutic opportunities, Nat. Rev. Drug Discov. (2013), https://doi.org/10.1038/nrd3978.
[10] S. Fais, L. O'Driscoll, F.E. Borras, E. Buzas, G. Camussi, F. Cappello, et al., Evidence-based clinical use of nanoscale extracellular vesicles in nanomedicine, ACS Nano 10 (2016) 3886–3899, https://doi.org/10.1021/acsnano.5b08015.
[11] O.P.B. Wiklander, M. Brennan, J. Lötvall, X.O. Breakefield, S.E.L. Andaloussi, Advances in therapeutic applications of extracellular vesicles, Sci. Transl. Med. (2019), https://doi.org/10.1126/scitranslmed.aav8521.
[12] J.P.K. Armstrong, M.N. Holme, M.M. Stevens, Re-engineering extracellular vesicles as smart nanoscale therapeutics, ACS Nano (2017), https://doi.org/10.1021/acsnano.6b07607.
[13] C. Montis, A. Zendrini, F. Valle, S. Busatto, L. Paolini, A. Radeghieri, et al., Size distribution of extracellular vesicles by optical correlation techniques, Colloids Surf. B Biointerfaces (2017), https://doi.org/10.1016/j.colsurfb.2017.06.047.
[14] C. Montis, S. Busatto, F. Valle, A. Zendrini, A. Salvatore, Y. Gerelli, et al., Biogenic supported lipid bilayers from nanosized extracellular vesicles, Adv. Biosyst. 2 (2018) 1700200, https://doi.org/10.1002/adbi.201700200.
[15] C. Montis, Y. Gerelli, G. Fragneto, T. Nylander, P. Baglioni, D. Berti, Nucleolipid bilayers: A quartz crystal microbalance and neutron reflectometry study, Colloids Surf. B Biointerfaces 137 (2016), https://doi.org/10.1016/j.colsurfb.2015.07.039.
[16] R. Vescovi, M. Monti, D. Moratto, L. Paolini, F. Consoli, L. Benerini, et al., Collapse of the plasmacytoid dendritic cell compartment in advanced cutaneous melanomas by components of the tumor cell secretome, Cancer Immunol. Res. (2019), https://doi.org/10.1158/2326-6066.CIR-18-0141.
[17] S. Busatto, A. Giacomini, C. Montis, R. Ronca, P. Bergese, Uptake profiles of human serum exosomes by murine and human tumor cells through combined use of colloidal nanoplasmonics and flow cytofluorimetric analysis, Anal. Chem. 90 (2018) 7855–7861, https://doi.org/10.1021/acs.analchem.7b04374.
[18] A. Zendrini, L. Paolini, S. Busatto, A. Radeghieri, M. Romano, M.H.M. Wauben, et al., Augmented COlorimetric NANoplasmonic (CONAN) method for grading purity and determine concentration of EV microliter volume solutions, Front. Bioeng. Biotechnol. (2020), https://doi.org/10.3389/fbioe.2019.00452.
[19] A. Mallardi, N. Nuzziello, M. Liguori, C. Avolio, G. Palazzo, Counting of peripheral extracellular vesicles in multiple sclerosis patients by an improved nanoplasmonic assay and dynamic light scattering, Colloids Surf. B Biointerfaces 168 (2018) 134–142, https://doi.org/10.1016/j.colsurfb.2018.02.006.
[20] L. Wang, J. Luo, Q. Fan, Monodispersed core-shell Fe3O4@ Au nanoparticles, J. Phys. Chem. B. 109 (2005) 21593–21601.
[21] M.L. Ainalem, R.A. Campbell, T. Nylander, Interactions between DNA and poly (amido amine) dendrimers on Silica surfaces, Langmuir 26 (2010) 8625–8635, https://doi.org/10.1021/la9047177.
[22] M. Rodahl, F. Höök, C. Fredriksson, C.A. Keller, A. Krozer, P. Brzezinski, et al., Simultaneous frequency and dissipation factor QCM measurements of biomolecular adsorption and cell adhesion, Faraday Discuss. (1997) 229–246, https://doi.org/10.1039/a703137h.
[23] C. Montis, Y. Gerelli, G. Fragneto, T. Nylander, P. Baglioni, D. Berti, Nucleolipid bilayers: A quartz crystal microbalance and neutron reflectometry study, Colloids Surf. B Biointerfaces 137 (2016) 203–213, https://doi.org/10.1016/j.colsurfb.2015.07.039.
[24] B. Gumí-Audenis, L. Costa, L. Redondo-Morata, P.E. Milhiet, F. Sanz, R. Felici, et al., In-plane molecular organization of hydrated single lipid bilayers: DPPC: cholesterol, Nanoscale 10 (2018) 87–92, https://doi.org/10.1039/c7nr07510c.
[25] B. Gumí-Audenis, F. Carlà, M.V. Vitorino, A. Panzarella, L. Porcar, M. Boilot, et al., Custom AFM for X-ray beamlines: In situ biological investigations under physiological conditions, J. Synchrotron Radiat. (2015), https://doi.org/10.1107/S1600577515016318.
[26] R.S. Armen, O.D. Uitto, S.E. Feller, Phospholipid component volumes: Determination and application to bilayer structure calculations, Biophys. J. 75 (1998) 734–744, https://doi.org/10.1016/S0006-3495(98)77563-0.
[27] A. Antosova, Z. Gazova, D. Fedunova, E. Valusova, E. Bystrenova, F. Valle, et al., Anti-amyloidogenic activity of glutathione-covered gold nanoparticles, Mater. Sci. Eng. C. 32 (2012) 2529–2535, https://doi.org/10.1016/j.msec.2012.07.036.
[28] A. Ridolfi, M. Brucale, C. Montis, L. Caselli, L. Paolini, A. Borup, et al., AFM-based high-throughput nanomechanical screening of single extracellular vesicles, BioRxiv. (2019), https://doi.org/10.1101/854539.
[29] M. Raudino, G. Selvolini, C. Montis, M. Baglioni, M. Bonini, D. Berti, et al., Polymer films removed from solid surfaces by nanostructured fluids: Microscopic mechanism and implications for the conservation of cultural heritage, ACS Appl. Mater. Interfaces 7 (2015), https://doi.org/10.1021/acsami.5b00534.
[30] M. Notarangelo, C. Zucal, A. Modelska, I. Pesce, G. Scarduelli, C. Potrich, et al., Ultrasensitive detection of cancer biomarkers by nickel-based isolation of polydisperse extracellular vesicles from blood, EBioMedicine (2019), https://doi.org/10.1016/j.ebiom.2019.04.039.
[31] B. Klasczyk, V. Knecht, R. Lipowsky, R. Dimova, Interactions of alkali metal chlorides with phosphatidylcholine vesicles, Langmuir (2010), https://doi.org/10.1021/la103631y.
[32] A. Nelson, Co-refinement of multiple-contrast neutron/X-ray reflectivity data using MOTOFIT, J. Appl. Crystallogr. 39 (2006) 273–276, https://doi.org/10.1107/S0021889806005073.
[33] A.H. Bahrami, R. Lipowsky, T.R. Weikl, The role of membrane curvature for the wrapping of nanoparticles, Soft Matter 12 (2015) 581–587, https://doi.org/10.1039/C5SM01793A.
[34] C. Montis, V. Generini, G. Boccalini, P. Bergese, D. Bani, D. Berti, Model lipid bilayers mimic non-specific interactions of gold nanoparticles with macrophage plasma membranes, J. Colloid Interface Sci. 516 (2018) 284–294, https://doi.org/10.1016/j.jcis.2018.01.064.
[35] C.M. Beddoes, C.P. Case, W.H. Briscoe, Understanding nanoparticle cellular entry: A physicochemical perspective, Adv. Colloid Interface Sci. 218 (2015) 48–68, https://doi.org/10.1016/j.cis.2015.01.007.
[36] T. Pfeiffer, A. De Nicola, C. Montis, F. Carlà, N.F.A. Van Der Vegt, D. Berti, et al., Nanoparticles at biomimetic interfaces: combined experimental and simulation study on charged gold nanoparticles/lipid bilayer interfaces, J. Phys. Chem. Lett. 10 (2019) 129–137, https://doi.org/10.1021/acs.jpclett.8b03399.
[37] E. Rascol, J.-M. Devoisselle, joel c Chopineau, The relevance of membrane models to understand nanoparticles-cell membrane interactions, Nanoscale 8 (2016) 4780–4798, https://doi.org/10.1039/C5NR07954C.
[38] A.H. Bahrami, M. Raatz, J. Agudo-Canalejo, R. Michel, E.M. Curtis, C.K. Hall, et al., Wrapping of nanoparticles by membranes, Adv. Colloid Interface Sci. 208 (2014) 214–224, https://doi.org/10.1016/j.cis.2014.02.012.
[39] R. Michel, M. Gradzielski, Experimental aspects of colloidal interactions in mixed systems of liposome and inorganic nanoparticle and their applications, Int. J. Mol. Sci. 13 (2012) 11610–11642, https://doi.org/10.3390/ijms130911610.